frontiers | Frontiers in Earth Science

TYPE Original Research
PUBLISHED 08 August 2022
DOI 10.3389/feart.2022.929597

OPEN ACCESS

EDITED BY
Daoyang Yuan,
Lanzhou, China

REVIEWED BY
Jia Cheng,
Ministry of Emergency Management, China
Yongge Wan,
Institute of Disaster Prevention, China

*CORRESPONDENCE
Lei Liu,
liulei41325@163.com

SPECIALTY SECTION
This article was submitted to Structural Geology and Tectonics, a section of the journal Frontiers in Earth Science

RECEIVED 27 April 2022
ACCEPTED 08 July 2022
PUBLISHED 08 August 2022

CITATION
Liu L, Zhuang W, Ji L, Zhu L and Jiang F (2022), Fault locking of the Qilian–Haiyuan fault zone before the 2022 Menyuan M_S6.9 earthquake and its seismic hazards in the future. *Front. Earth Sci.* 10:929597. doi: 10.3389/feart.2022.929597

Fault locking of the Qilian–Haiyuan fault zone before the 2022 Menyuan M_S6.9 earthquake and its seismic hazards in the future

Lei Liu*, Wenquan Zhuang, Lingyun Ji, Liangyu Zhu and Fengyun Jiang

The Second Monitoring and Application Center of China Earthquake Administration, Xi'an, China

By using GPS-derived velocities of 2015–2021 and a negative dislocation program, we inverted the locking degree and slip rate deficit in the Qilian–Haiyuan fault zone, and combined with the distribution of small earthquakes in the fault, we studied the characteristics before the 2022 Menyuan M_S6.9 earthquake and analyzed the future seismic hazards of each segment within this fault zone. The regional crustal deformation pattern is discussed with regard to the fault slip rate and regional strain rate field. The preliminary results show that before the earthquake, the seismogenic fault was strong locked, with a high locking depth, the slip rate deficit was large, and the distribution of small earthquakes was relatively few, these characteristics are closely related to the occurrence of strong earthquakes, according to the aftershock relocation results, further, it is believed that the earthquake may link the Lenglongling and Tuolaishan faults into a large strike-slip fault. The Jinqianghe fault, the Lenglongling fault, and the eastern segment of the Tuolaishan fault are strongly locked, with high locking depth and large slip rate deficit, combined with the occurrence of small earthquakes and the locking degree before the 2022 Menyuan M_S6.9 earthquake, indicate that the eastern segment of the Tuolaishan fault is highly likely to have strong earthquakes in the future, which requires further attention. In addition, the strike-slip rate of the Qilian–Haiyuan fault zone is mainly between 3.9 and 4.3 mm/yr, the overall movement of the fault is consistent, and the compressional rate gradually decreases from 2.9 mm/yr in the western segment to 1 mm/yr in the eastern segment; the fault compressional rate may be related to the crustal shortening (formation basin and uplift mountain). Therefore, the present-day crustal deformation in the northeastern margin of the Tibetan Plateau is mainly distributed in the shortened region of the crust on the Qilian Shan area and left-lateral strike-slip localized on the Qilian–Haiyuan fault zone.

KEYWORDS

Qilian-Haiyuan fault zone, Menyuan M_S6.9 earthquake, fault locking, seismic hazard, crustal deformation

1 Introduction

The northeastern margin of the Tibetan Plateau belongs to the Qaidam–Qilian active block (Zhang et al., 2003), which is the front part of the expansion of the Tibetan Plateau to the interior of the continent. It absorbs and modulates the NNE compression and convergence of the Indian plate to the Eurasian plate and has strong tectonic activity, causing the occurrence of relatively frequent moderate and strong earthquakes (Dewey and Burke, 1973; Métivier et al., 1998; Zhang et al., 2004; Molnar and Stock, 2009). The Qilian–Haiyuan fault zone is a large strike-slip fault zone in the northeastern margin of the Tibetan Plateau, this fault not only controls the geometry and tectonic pattern of the northeastern margin of the Tibetan Plateau, but also plays an important role in regulating the eastward movement of crustal material in the northeastern margin relative to the Alashan block. The fault zone is mainly left-lateral strike-slip, with a total length of approximately 1,000 km, and is mainly composed of the Tuolaishan, Lenglongling, Jinqianghe, Maomaoshan, Laohushan, and Haiyuan faults from west to east (Tapponnier and Molnar, 1976; Peltzer and Tapponnier, 1988; Gaudemer et al., 1995; Tapponnier et al., 2001; Zheng et al., 2013; Daout et al., 2016). Currently, faults are highly seismically active. According to historical records, there have been several moderate and strong earthquakes in the Qilian–Haiyuan fault zone since 1900, such as the 1920 Haiyuan *M*8.5, 1986 Menyuan *M*6.4, 1990 Tianzhu *M*6.2, and 2016 Menyuan M_S6.4 earthquakes. In addition, the Menyuan M_S6.9 earthquake (8 January 2022) also occurred in the Tuolaishan and Lenglongling faults (Li et al., 2022; Yang et al., 2022). According to the Global Centroid Moment Tensor (GCMT) inversion results, the epicenter was located at 37.80°N and 101.31°E, with a focal depth of 14.8 km (https://www.globalcmt.org/CMTsearch.html), and the focal mechanism was a high-angle left-lateral strike-slip fault. This shows that the Qilian–Haiyuan fault zone controlled a series of historical earthquakes and is a natural testing ground for studying the mechanism of earthquake initiation (Figure 1).

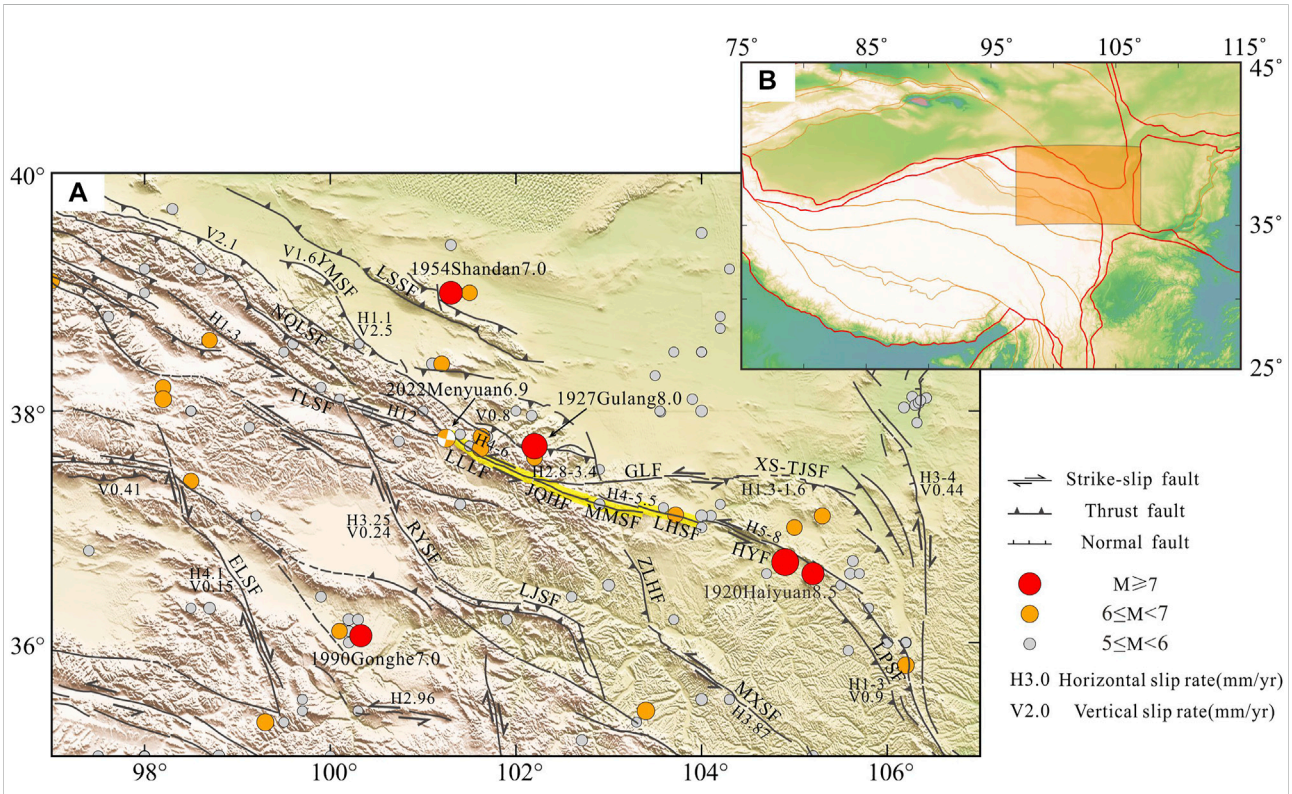

FIGURE 1
(A) Active faults and earthquakes in the northeastern margin of the Tibetan Plateau. Black lines represent fault lines mapped by (Xu et al., 2017). Gray, orange, and red circles indicate the locations of *M*5 ~ 6, *M*6 ~ 7, and ≥*M*7 earthquakes that have occurred since 1900, respectively. The focal mechanism solutions were obtained from Global CMT Catalog (http://www.globalcmt.org/CMTsearch.html). Yellow line follows the Tianzhu seismic gap (Gaudemer et al., 1995). The Geologic slip rate from Yuan et al. (2004). LSSF: Longshoushan fault; YMSF: Yumushan fault; NQLSF: Northern Qilian Shan fault; TLSF: Tuolaishan fault; LLLF: Lenglongling fault; JQHF: Jinqianghe fault; MMSF: Maomaoshan fault; LHSF: Laohushan fault; HYF: Haiyuan fault; GLF: Gulang fault; XS–TJSF: Xiangshan–Tianjingshan fault; LPSF: Liupanshan fault; ELSF: Elashan fault; RYSF: Riyueshan fault; LJSF: Lajishan fault; ZLHF: Zhuanglanghe fault; MXSF: Maxianshan fault **(B)** Location of the study area in relation to the Tibetan Plateau. The orange box is the area shown in **(A)**. The orange lines are active block boundaries mapped by Zhang et al. (2003).

Earthquake occurrences are closely related to fault activity. Strong and large earthquakes often occur in fault-locked segments or asperities with high strain accumulation in the active fault zone (Wiemer and Wyss, 1997; Wyss and Wiemer, 2000). The inversion of the fault locking degree and slip rate deficit based on geodesic observation data can facilitate the identification of fault asperities and study fault seismogenic capacity. For example, after the Wenchuan M_S8.0 earthquake in 2008, the locking degree of the Longmen Shan fault was already in high at the source before the earthquake, but it was adjusted to non-locking after the earthquake (Zhao et al., 2012, 2020). After the Chile M_W8.8 earthquake in 2010, Madariaga et al. (2010) predicted that a large earthquake would occur in this region 10 years ago, mainly based on the strong locking of the fault and rupture gap of the strong earthquake (Moreno et al., 2010). The strong locking of the Japan Trench fault before the M_W9.0 earthquake of 2011 in Japan, based on GPS data was essentially consistent with the coseismic dislocation concentration area of this earthquake in space (Hashimoto et al., 2009; Loveless and Meade, 2011). The source of the 2015 M_W7.8 earthquake in Nepal was located at the edge of the strong locked fault, and between the rupture zone of the Karnali M8.2 earthquake in 1,505 and the Bihar M8.1earthquake in 1934 (Zhao et al., 2017). Therefore, the locking degree and slip rate deficit characteristics of faults are important for predicting the seismic hazards of the fault zone (McCaffrey, 2005; McCaffrey et al., 2007; Cavalié et al., 2008; Jolivet et al., 2013).

Thus far, extensive research on the seismic hazards of the Qilian–Haiyuan fault zone has been performed. Using field investigations and remote-sensing images, Gaudemer et al. (1995) found that there was a 220 km long earthquake hazard zone–"Tianzhu seismic gap" on the Qilian–Haiyuan fault zone. Using field geological investigations, Guo (2019) considered that the 160 km long zones of the eastern segment of the Jinqianghe, Maomaoshan, and Laohushan faults may experience large earthquakes in the future. Hao et al. (2017) used GPS data to invert the locking degree of the Haiyuan–Liupanshan fault and analyzed the areas where strong earthquakes may occur in the future. Moreover, Li et al. (2014) and Li et al. (2016) performed inversion of the locking of the Qilian–Haiyuan–Liupanshan fault zone and believed that the Jinqianghe–Maomaoshan fault had a high seismic hazard. Therefore, the Qilian–Haiyuan fault zone is still the focus of strong earthquakes, and the Menyuan M_S6.9 earthquake in 2022 has once again made us realize the strong seismicity of the Qilian–Haiyuan fault zone. Are there any abnormal characteristics before the earthquake? How will this affect the seismic hazard of faults in the future? These problems are of great significance for future seismic potential assessments of fault zones and require further analyses.

In this paper, we examined the Qilian–Haiyuan fault zone as the research object, utilizing the GPS velocity field results from 2015 to 2021, the strain rate field of the region and slip rates of major faults were obtained. Further, the locking degree and slip rate deficit of the fault zone were inverted, and combined with the regional relocation of small earthquakes and the relocation of the aftershocks of the 2022 Menyuan M_S6.9earthquake, the present-day activity and characteristics of small earthquakes occurring within this fault zone were comprehensively analyzed. Subsequently, according to the characteristics of this fault zone before the Menyuan M_S6.9 earthquake, the segments of the fault where strong earthquakes may occur in the future are determined. Finally, the regional crustal deformation pattern is discussed with regard to the strain rate field and fault slip rate, for the regions for which strong seismic hazard prediction and the tectonic transformation pattern of the northeastern margin of the Tibetan Plateau, to provide appropriate references and constraints.

2 Faults slip rate and strain rate field

2.1 GPS data processing

We collected GNSS observation data from the Crustal Movement Observation Network of China (CMONOC I/II) from 2015 to 2021. We adopted a strategy to uniformly process/reprocess daily GPS data using the GAMIT software (Herring et al., 2015) to ensure the quality and homogeneity of the solutions. The main methods used are as follows: The baseline calculation of the GNSS observation data was carried out using a single day as one period. In addition to allowing the slight adjustment of satellite orbit and Earth rotation parameters, we used the gravity field model EGM08, optical pressure model BERNE, Earth radiation model TUME1, antenna inference model ANTBK, geomagnetic field model IGRF13, and high–order ionospheric correction model GMAP to estimate and correct the relevant parameters in data processing.

To avoid the differences in calculation results caused by the difference between the model and frame, the same model and method were used to process the data from approximately 70 IGS stations and reference stations selected globally with a uniform distribution and obtain the baseline relaxation solution. HTOGLB was then used to convert the single-day relaxation solution files into GLOBK-approved single-day baseline relaxation solutions. Furthermore, GLRED was used to calculate the coordinate time series under the ITRF 2014 (Altamimi et al., 2017). The repeatability of the day coordinates was then checked. Finally, the seasonal variation of annual and half-yearly cycles, the step caused by instrument replacement, and other nonstructural factors were removed by model fitting. Next, the GNSS velocity field under the

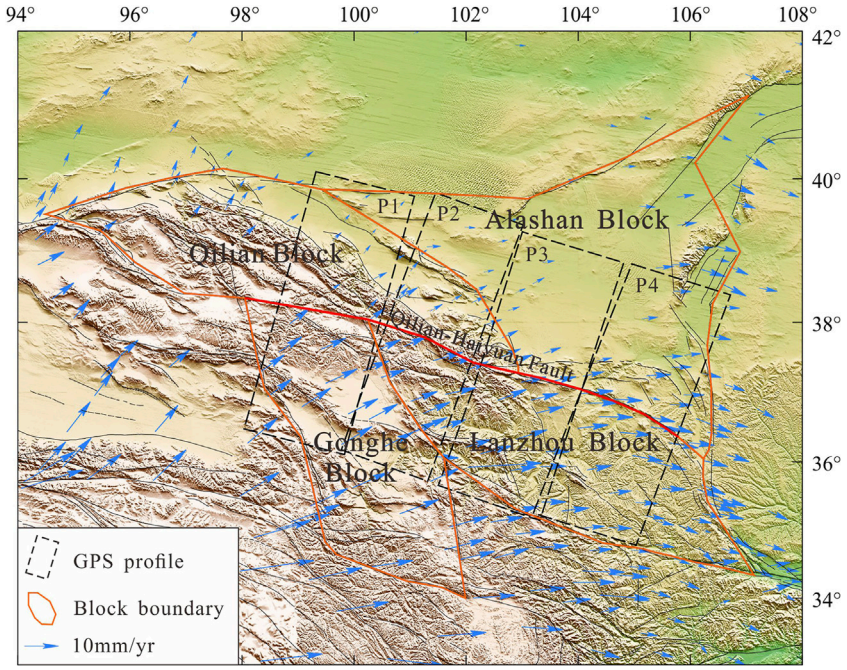

FIGURE 2
GPS horizontal velocity fields and block boundaries. The red line indicates the Qilian–Haiyuan fault zone. The orange lines indicate active block boundaries. Blue arrows represent the GPS horizontal velocities with respect to stable Eurasia plate. Black dotted rectangles show the locations of GPS horizontal velocity profiles in Figure 3.

ITRF2014 framework was estimated from the clean time series of many years; using the Euler rotation vector between the Eurasian frame (provided by Altamimi et al. (2017)) and ITRF 2014, the GNSS horizontal motion velocity field into the stable Eurasian reference frame was calculated. At the same time, the measurement stations in the GNSS velocity field that deviated significantly from the direction and size of the research region were removed (Figure 2).

2.2 GPS velocity profiles

The GPS velocity profile of the fault can directly reflect the differential motion of the blocks on both sides and the strain accumulation state of the fault (Wang and Shen, 2020; Song et al., 2022). Therefore, to study the current slip rate of the Qilian–Haiyuan fault zone and the regional differential motion characteristics, we constructed four profiles from west to east across the Qilian–Haiyuan fault zone (profiles P1, P2, P3, and P4 in Figure 2). The GPS horizontal velocity field was projected along the fault strike direction and normal fault strike direction, the strike-slip rate or extensional/compressional rate of the fault was estimated from the difference between the average velocities of two stations on both sides of the fault, and the error propagation law was used to calculate the rate error (Figure 3; parallel fault rates on the left and normal fault rates on the right). Profile P1 mainly includes the Elashan, Tuolaishan, the Northern Qilian Shan, and Yumushan faults. It can be seen that the Tuolaishan fault is given priority to with left-lateral strike-slip, and compressional movement, has a strike-slip rate of 4.0 mm/yr and a compressional rate of 2.9 mm/yr. The Northern Qilian Shan and Yumushan faults also have the left-lateral strike-slip and compressional movement, however, their fault activity is weak and the slip rate is about 1 mm/yr. Profile P2 mainly includes the Riyueshan, Lenglongling, the Northern Qilian Shan, and Longshoushan faults. The Lenglongling fault has a left-lateral strike-slip rate of 3.9 mm/yr and a compressional rate of 2.2 mm/yr. The Riyueshan fault has no obvious strike-slip and a compressional rate of 2.2 mm/yr, while the Longshoushan fault mainly shows thrusting deformation and has a compressional rate of 1.9 mm/yr. Profile P3 mainly includes the Lajishan and the Jinqianghe–Maomaoshan–Laohushan faults. The Jinqianghe–Maomaoshan–Laohushan fault has a strike-slip rate of 3.9 mm/yr and a compressional rate of approximately 1.3 mm/yr. The Lajishan fault has weak strike-slip and extensional effects. Profile P4 includes the Maxianshan, Haiyuan, and Xiangshan–Tianjingshan faults, which have a left-lateral strike-slip rate of 4.3 mm/yr and a compressional

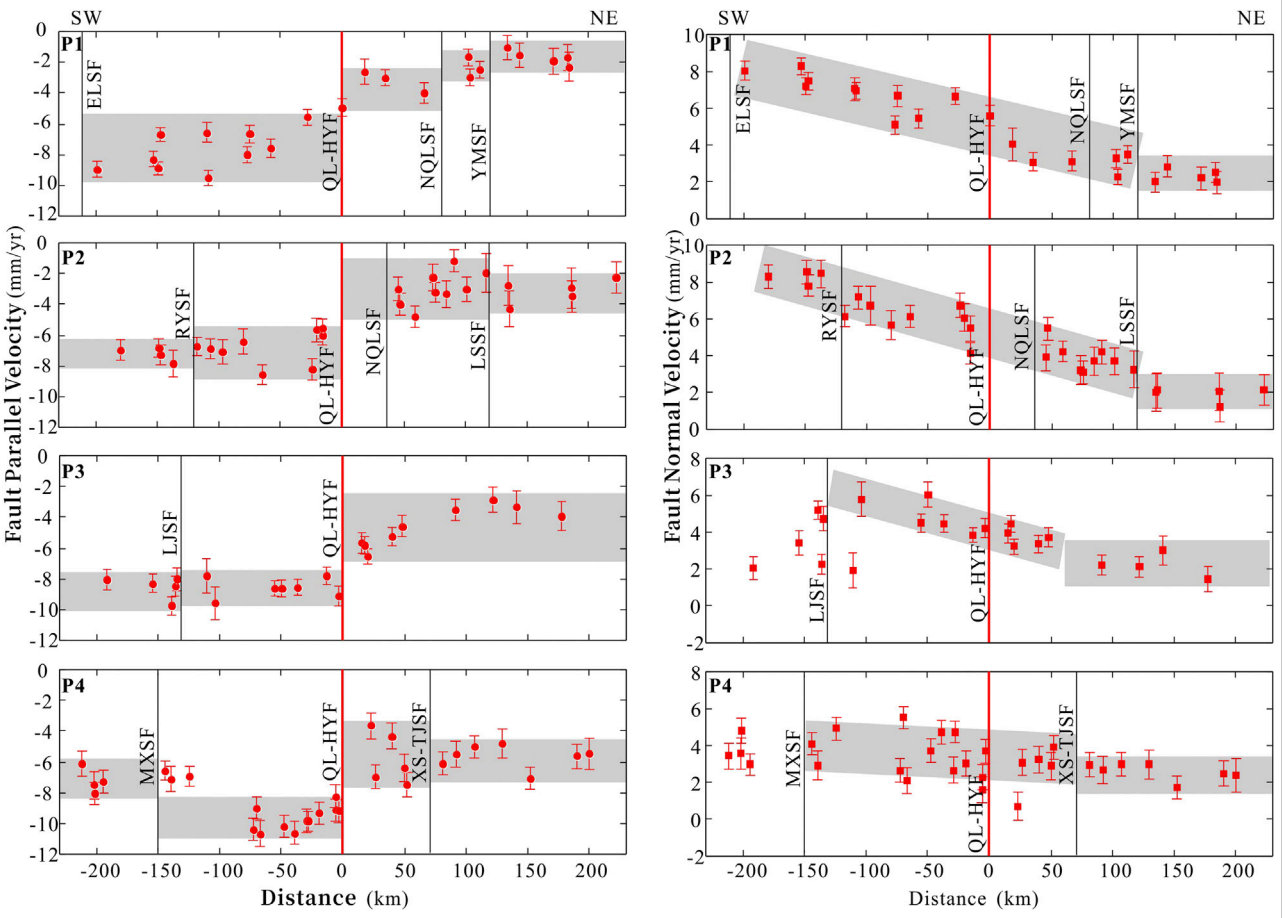

FIGURE 3
GPS horizontal velocity profile across the faults. Locations of each profile are shown in Figure 2. Red bars denote ranges of velocity measurements. Red line marks the Qilian–Haiyuan fault, while the black line marks other fault. Charts on the left are parallel velocities of the fault along the four profiles across the fault. Charts on the right are normal velocities. The middle value in the gray rectangle is used to determine slip rate of fault.

rate of approximately 1 mm/yr. However, the Maxianshan and Xiangshan–Tianjingshan faults are not active at present and have weak strike-slip and compression rates.

In the whole region, it can be seen that profiles P1 and P2 cross the whole Qilian Shan region, and the profiles from SW to NE exhibit left-lateral strike-slip with thrusting deformation. The velocity changes along parallel faults were mainly concentrated on both sides of the faults, and the velocity changes along normal faults were linear gradients. The total crustal shortening rate is 6–7 mm/yr. This shortening is distributed throughout the Qilian Shan across a width of 200–250 km, the linear velocity gradient suggests relative homogeneous convergence across the whole mountains rather than major slip on a particular faults or structures, which supports the "continuous deformation model" of the Tibetan Plateau (England and Houseman, 1986). In profiles P3 and P4, the region mainly showed a left-lateral strike-slip, and compression shortening was not evident. The velocity step along the parallel fault direction is concentrated on the Qilian–Haiyuan fault, with a width of 50 km. The fault normal velocity is weakened in profile P3, the crustal shortening rate is reduced to 3 mm/yr and the width is reduced to 150 km. The faults in profile P4 are almost non-compression, and the crustal shortening rate of the entire profile is only 1–2 mm/yr. In addition, it can be seen from the four profiles that the parallel and normal fault velocities of the GPS in the Alashan block are basically unchanged.

2.3 Strain rate field

The spatial inconsistency of the GPS horizontal velocity field is a direct reflection of crustal deformation, and the

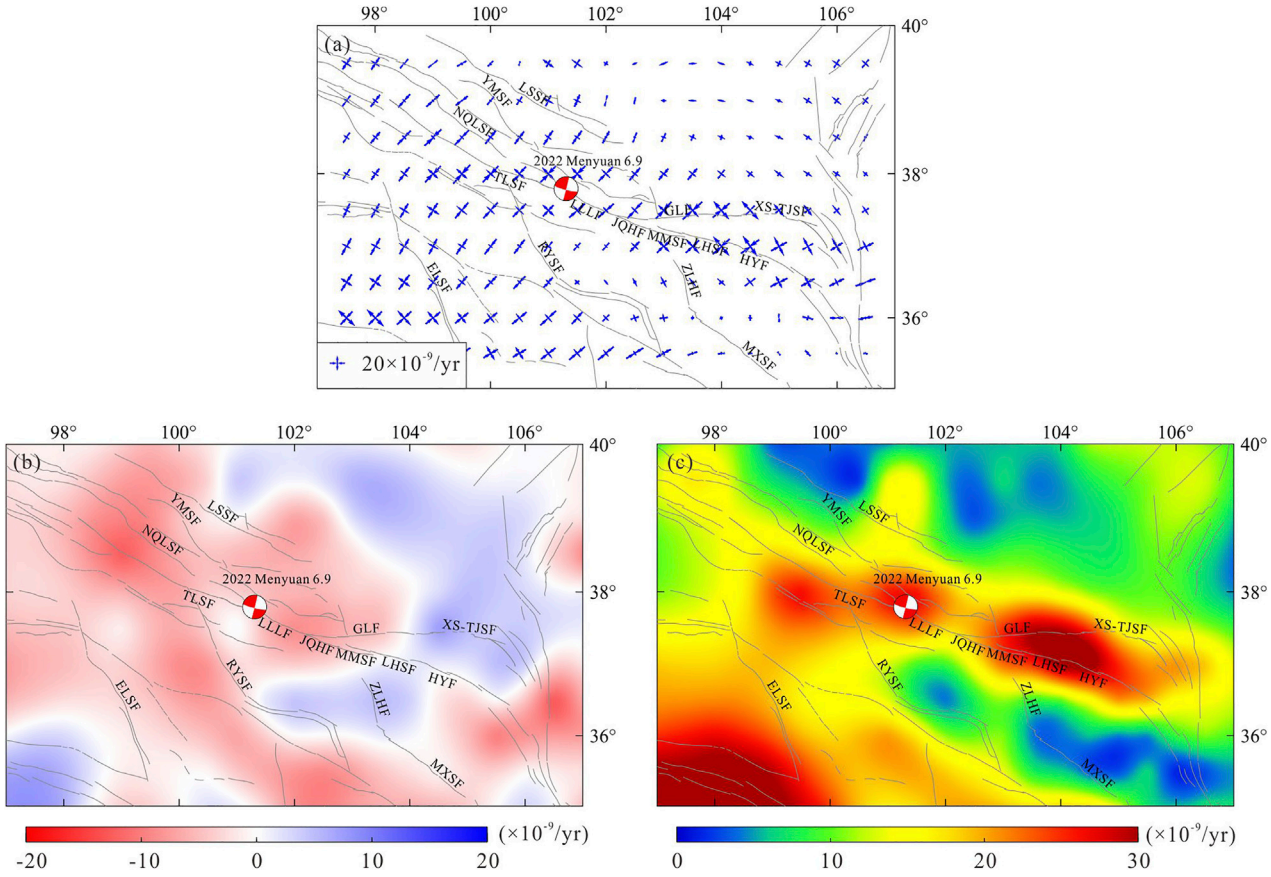

FIGURE 4
Principal strain rate **(A)** dilatation rate **(B)** and maximum shear strain rate **(C)** of the study area. LSSF: Longshoushan fault; YMSF: Yumushan fault; NQLSF: Northern Qilian Shan fault; TLSF: Tuolaishan fault; LLLF: Lenglongling fault; JQHF: Jinqianghe fault; MMSF: Maomaoshan fault; LHSF: Laohushan fault; HYF: Haiyuan fault; GLF: Gulang fault; XS–TJSF: Xiangshan–Tianjingshan fault; LPSF: Liupanshan fault; ELSF: Elashan fault; RYSF: Riyueshan fault; LJSF: Lajishan fault; ZLHF: Zhuanglanghe fault; MXSF: Maxianshan fault.

strain–rate field is an important index for describing regional deformation. This index is not affected by the reference frame and can reflect the regional deformation characteristics at different resolutions (Yang et al., 2002; Meng et al., 2009). To visualize the crustal deformation of the studied region, we calculated the strain rate field using the continuous function method developed by Shen et al. (2015). This method interpolates a set of discrete GPS velocities and introduces a spatial weighting function with a smoothing distance optimally determined according to the *in situ* data quality. It is robust because it does not depend on certain assumptions regarding the data. As shown in Figure 4A, the results of the principal strain rate show that the crust rotates clockwise along the northeastern margin of the Tibetan Plateau, and the orientation of the principal compressional strain rate is mainly NE-NEE. The principal strain rate is larger along the Qilian–Haiyuan fault zone, and the extensional strain increases gradually from west to east, while the principal strain rate in the Alashan block is smaller. The dilatation rate (Figure 4B) shows that it is mainly compressional in the Qilian Shan, changes to extension east of the Maomaoshan fault, and then changes to compression in the surrounding area of Liupanshan. There was also a weak extension in the Alashan block. The maximum shear strain rate (Figure 4C) shows that there is an area with a high shear strain along the Qilian–Haiyuan fault zone, which is consistent with the conclusion that the fault is mainly strike-slip. The strain rate field corresponded well with the GPS profile. The strike-slip movement is evident in the Qilian–Haiyuan fault zone, and the compression movement gradually weakens on both sides of the fault zone from west to east. In addition, before the 2022 Menyuan M_S6.9 earthquake, the dilatation rate at the seismogenic location was small, whereas the maximum shear strain rate was high (24×10^{-9}/yr), which was consistent with the left-lateral strike-slip being the focal mechanism of this earthquake.

3 Fault locking degree and slip rate deficit on the Qilian–Haiyuan fault zone

3.1 Block Model

We used the negative dislocation inversion model, which assumes that GPS velocities are a combined effect of rotation, interseismic elastic strain from bounding fault locking, and horizontal strain within blocks (Eq. 1). The block rotation Euler pole, fault slip rate, and block boundary fault coupling coefficients (Phi) are retrieved by grid search and simulated annealing using a downhill simplex method. The model principle, inversion process, and parameter control have been introduced in a previous study (McCaffrey, 2009). The modeling was implemented using the open-source TDEFNODE software (McCaffrey, 2009). The quality of model parameter fitting is represented by Eq. 2, when χ_n^2 approaches 1, the model is considered to represent the best-fitting observation data (McCaffrey, 2002).

$$\bar{V}_{sf} = \bar{V}_{br} + \bar{V}_{is} + \bar{V}_{fs} \tag{1}$$

Herein, $\bar{V}_{sf}$ is the measured surface velocity, $\bar{V}_{br}$ is the velocity caused by rotation of the blocks, $\bar{V}_{is}$ is the velocity caused by the internal strain of the blocks, and $\bar{V}_{fs}$ is the velocity caused by the negative dislocation effect of fault locking.

$$\chi_n^2 = \left[\sum_1^n (r_i / f\sigma_i)^2\right] \Big/ dof \tag{2}$$

Herein, r_i is the residual, σ_i is the standard deviation, f is the weight factor, and dof is the degrees of freedom (number of observations minus number of free parameters).

Our model was constructed as follows: The northeastern margin of the Tibetan Plateau is divided into four tectonic blocks based on the GPS velocities and geological and seismological evidence for active faulting (Zhang et al., 2003; Wang et al., 2011; Li et al., 2015): the Alashan, Lanzhou, Gonghe, and Qilian blocks (The orange lines in Figure 2). In our inversion, the Alashan block acted as rigid block (Zhang et al., 2005; Wang et al., 2009), while the other blocks underwent internal deformation. We removed the sites that were obviously different with regard to movement trend and size inside and around the block, and 153 GPS sites were selected to participate in the inversion. During the inversion, the simplified Qilian–Haiyuan fault zone was a single continuous fault with NWW strike and SSW dip and dip angles of 80°, 75°, and 70° from west to east. The fault plane was composed of horizontal and deep nodes. Along the strike of the Qilian–Haiyuan fault zone, the distance between the nodes was approximately 30 km, with a total of 26 nodes. Seven nodes were set in the depth direction and the distances were 0.1, 5, 10, 15, 20, 25, and 30 km. We also assume that the fault is fully locked at the surface (Phi = 1) and freely slips below a depth of 30 km (Phi = 0), with the Phi decreasing down-dip from 1 to 0 between 0.1 and 30 km at depth (McCaffrey, 2002; Wang et al., 2003).

3.2 Fault locking on the Qilian-Haiyuan fault zone

We present the fault locking (Figure 5) of the Qilian–Haiyuan fault zone for our best-fitting model on the basis of the parameter setting and inversion strategies described above. It can be seen that the Jinqianghe fault, the Lenglongling fault, and the eastern segment of the Tuolaishan fault are strongly locked; the locking depth of the Jinqianghe fault and the western segment of the Lenglongling fault is about 25 km. The 2022 Menyuan M_S6.9 earthquake occurred in the strongly locked area of the western segment of the Lenglongling Fault. The locking depth of the eastern segment of the Lenglongling fault is only 6 km, and the locking depth of the eastern segment of the Tuolaishan fault is 12–24 km. There is weak locked in the western segment of the Tuolaishan fault, with a locking depth of 6–15 km. However, the middle segments of the Tuolaishan, Maomaoshan, Laohushan, and Haiyuan faults are unlocked or weakly locked. They are weakly locked at the shallow part and show creep sliding below a depth of 5 km.

3.3 Slip rate deficit on the Qilian-Haiyuan fault zone

When the fault is locked, the slip rate deficit accumulates near the fault in the form of strain energy (McCaffrey et al., 2007). The slip rate deficit can indicate how fast the slip of the two sides of the fault is transformed into strain energy, which is of great significance to the judgment of fault-associated seismic hazards (Jolivet et al., 2013). The distribution of the slip rate deficit of the Qilian–Haiyuan fault zone (Figure 6) is consistent with the distribution of the fault locking, and the slip rate deficit gradually decreases from the shallow part to the deep part of the fault. In the eastern segment of the Tuolaishan fault, the slip rate deficit is 6–6.5 mm/yr and the depth is 12–24 km. The slip rate deficit of the western segment of the Lenglongling fault is 6 mm/yr and the depth is 25 km, while the slip rate deficit of the eastern segment is 5.5 mm/yr and the depth is only 6 km. The slip rate deficit of the Jinqianghe fault is 5–5.5 mm/yr and the depth is 25 km. However, in the middle and western segment of the Tuolaishan fault, the slip rate deficit is mainly 3–4 mm/yr, and only the depth of the middle-west segment reaches 15 km, while the rest of the fault is concentrated in the shallow surface of 5 km. The slip rate deficit of the Maomaoshan fault gradually decreases from 3 mm/yr in the shallow region to 1.7 mm/yr in the deep region. The slip rate deficit of the Laohushan and Haiyuan faults is about 3 mm/yr, only distributed in the shallow surface of 4 km, gradually changing to 0 mm/yr in the deep region.

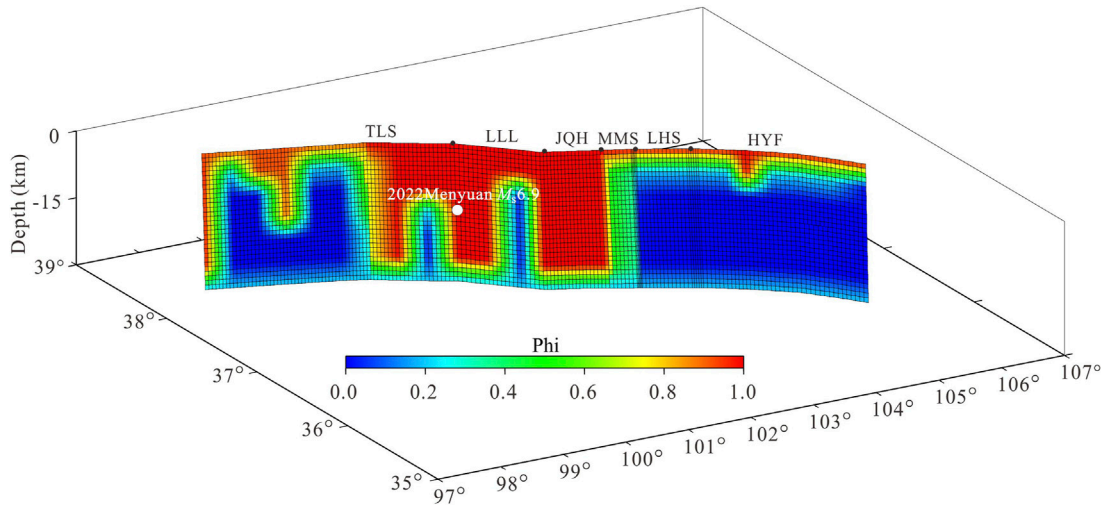

FIGURE 5
Locking degree of the Qilian–Haiyuan fault zone. Hypocenter parameters were obtained from Global CMT Catalog (http://www.globalcmt.org/CMTsearch.html). TLSF: Tuolaishan fault; LLLF: Lenglongling fault; JQHF: Jinqianghe fault; MMSF: Maomaoshan fault; LHSF: Laohushan fault; HYF: Haiyuan fault.

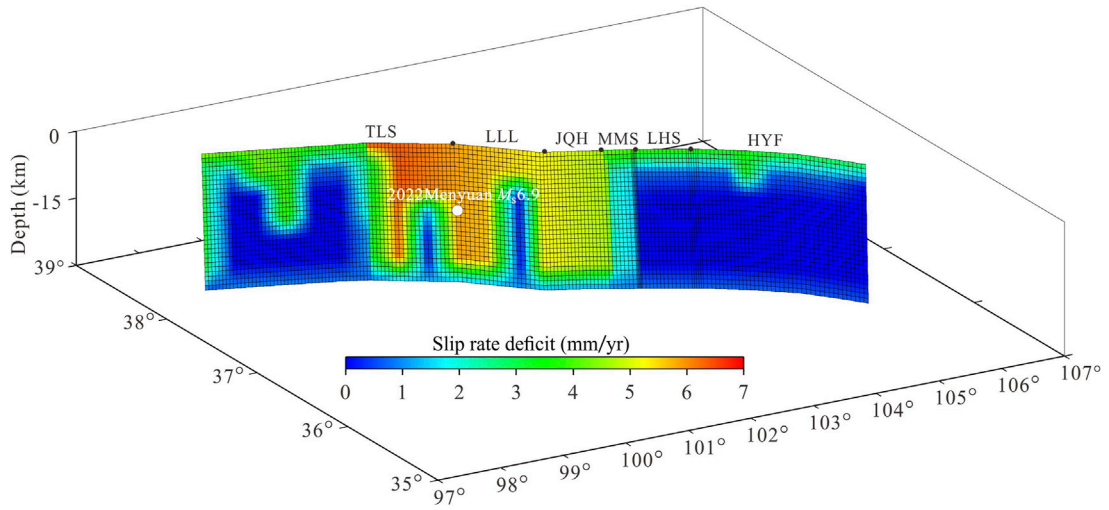

FIGURE 6
Slip rate deficit of the Qilian–Haiyuan fault zone. Hypocenter parameters were obtained from Global CMT Catalog (http://www.globalcmt.org/CMTsearch.html). TLSF: Tuolaishan fault; LLLF: Lenglongling fault; JQHF: Jinqianghe fault; MMSF: Maomaoshan fault; LHSF: Laohushan fault; HYF: Haiyuan fault.

4 Distribution of small earthquakes in the Qilian-Haiyuan fault zone

To study the relationship between the locking degree and small earthquakes of the Qilian–Haiyuan fault zone, based on the relocation catalog of small earthquakes with M_L1.5 and above during 2009–2019 provided by Mr. Long Feng of the Sichuan earthquake agency, the earthquakes occurring within 15 km on both sides of the fault strike were selected and projected onto the fault plane along the fault strike (Figure 7); it can be seen that the distribution of earthquakes on the Qilian–Haiyuan fault zone is dense and uneven in each segment of the fault. The locking depth

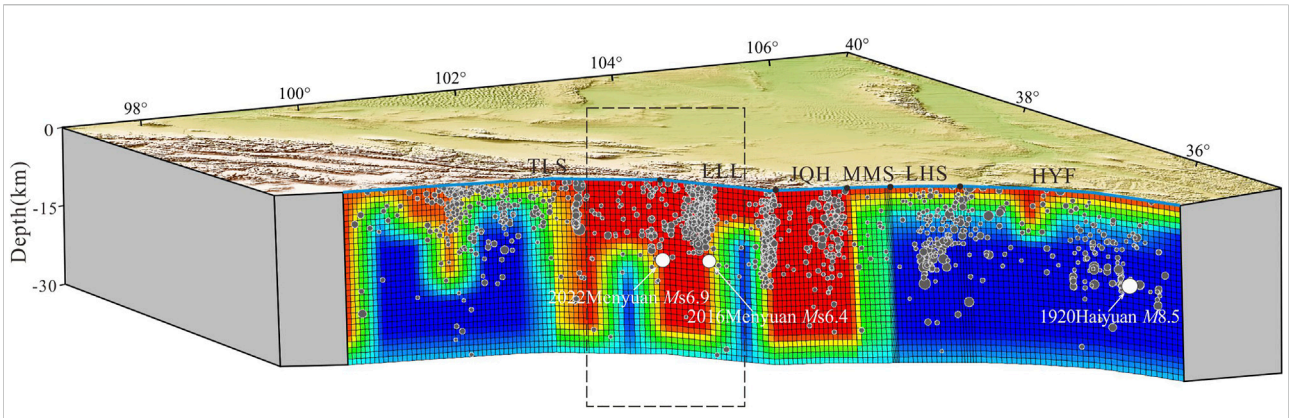

FIGURE 7
Locking degree and distribution of small earthquakes in the Qilian–Haiyuan fault zone. The white circles indicate the locations of the 1920 Haiyuan *M*8.5, 2016 Menyuan M_S6.4, and 2022 Menyuan M_S6.4 earthquakes. The gray circles are the relocation catalog of small earthquakes during 2009–2019. Black dotted rectangle shows the profile of small earthquakes in Figure 9. TLSF: Tuolaishan fault; LLLF: Lenglongling fault; JQHF: Jinqianghe fault; MMSF: Maomaoshan fault; LHSF: Laohushan fault; HYF: Haiyuan fault.

is consistent with the depth of small earthquakes, which indicates that the fault is locked at a depth of 25 km (Schmittbuhl et al., 2015; Li et al., 2020). In the middle and western segments of the Tuolaishan fault, the fault is weakly locked, the locking depth is shallow, and there are more small earthquakes, whereas in the eastern segment, the fault is strongly locked, the locking depth is deep, and the distribution of small earthquakes is lesser. The Lenglongling fault is strongly locked; the locking depth of its western segment is larger than that of its eastern segment, small earthquakes are concentrated in the middle-west segment of the fault, and the depth of this fault is more than 14 km. The 2016 Menyuan M_S6.4 earthquake occurred in this area, the occurrence of intensive small earthquakes here is related to the energy release of the 2016 Menyuan M_S6.4earthquake. The reason why the epicenter of this earthquake is in the strong locked area may be that because the GPS data (2015–2021) contain information regarding the 2016 Menyuan M_S6.4earthquake, they also reflect the characteristics of strong locked in this region before the earthquake. There are fewer earthquakes at the intersection of the Lenglongling fault and the Tuolaishan fault, and the 2022 Menyuan M_S6.9 earthquake occurred in this area, the two Menyuan earthquakes were located on the east and west sides of the strongly locked segment of the Lenglongling fault, which is well explained by the occurrence of strong earthquakes in the strongly locked segment of this fault. The impact of this earthquake on faults will be discussed in the next section. The Jinqianghe fault shows strong locked and a large locking depth. There are many small earthquakes in the eastern segment of this fault, at the intersection of the Jinqianghe and Lenglongling faults; these earthquakes are concentrated and distributed in the band at a depth of 18 km. This may be due to the strong tectonic activity at the intersection of the Gulang fault and the Qilian–Haiyuan fault, which makes the occurrence of earthquakes more likely (Gao, 2018; Liu et al., 2020). The locking degree of the Maomaoshan fault is approximately 0.5, the earthquake distribution is low. Further, the Laohushan fault is weakly locked and shows a shallow the locking depth, there are many small earthquakes with a depth of less than 18 km. The large number of earthquakes corresponds to the conclusion of a study by Jolivet et al. (2012), which reported that there is a creep segment in the Laohushan fault; The Haiyuan fault is weakly locked and shows a shallow locking depth. The frequency of the occurrence of small earthquakes was lower in the western segment and higher in the eastern segment, and the depth of the small earthquakes was approximately 18 km, which is consistent with the epicenter depth of the 1920 Haiyuan *M*8.5 earthquake (Zhan et al., 2004; Han et al., 2008). Since the 1920 Haiyuan *M*8.5 earthquake, which occurred in the southeastern segment of the Haiyuan fault, this fault may have been affected by the fault adjustment-associated movement after the earthquake, due to which many small earthquakes still occur in this region.

5 Discussion

5.1 Reliability analysis of results

The χ^2_n is the ratio of the variance of posterior unit weight to the variance of the anterior unit weight. The inversion result was better when the value was approximately 1. According to Eq. 2, it can be seen that the size of χ^2_n is related to the weight factor *f*, which ranges from 1 to 5 for the GPS horizontal velocity field data error (Mao et al., 1999). In the inversion, the value of χ^2_n can be adjusted as close to 1 as possible by gradually changing the size of *f*, via a large number of test

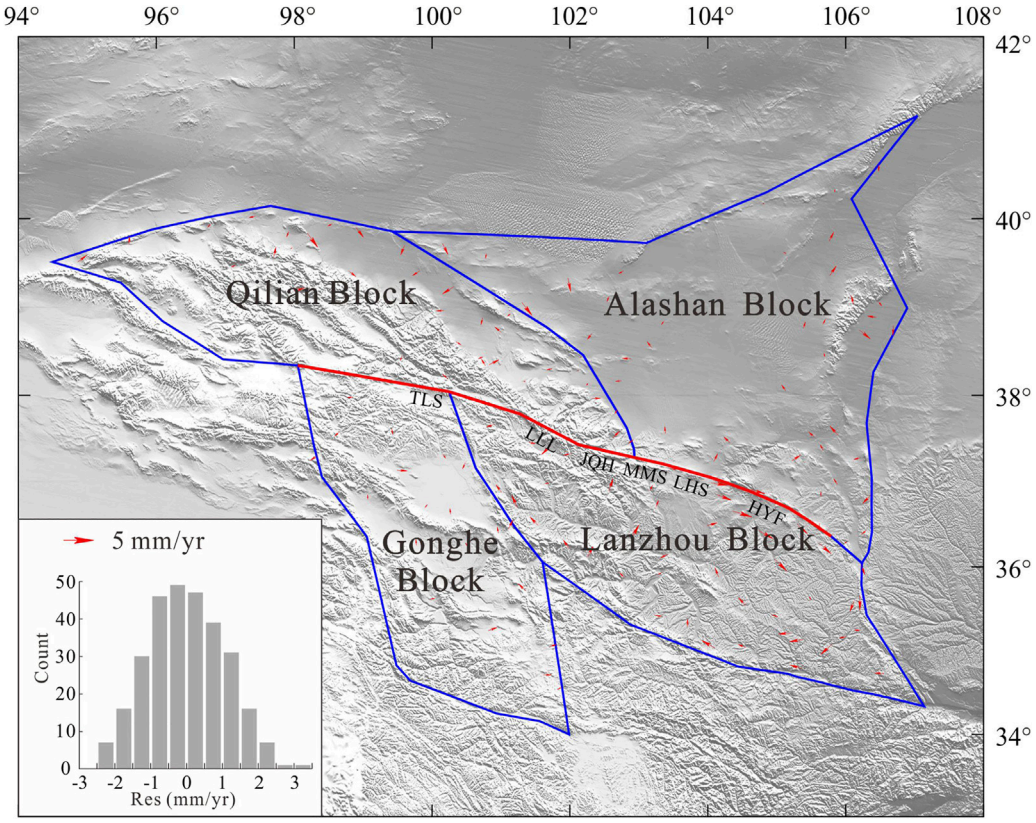

FIGURE 8
GPS velocity residuals associated with the block kinematic model and their statistical histogram. The red line is the Qilian–Haiyuan fault zone. The blue lines are active block boundaries. Red arrows represent the GPS velocities residuals. TLSF: Tuolaishan fault; LLLF: Lenglongling fault; JQHF: Jinqianghe fault; MMSF: Maomaoshan fault; LHSF: Laohushan fault; HYF: Haiyuan fault.

calculations, we found that when the weight factor $f = 3.9$, $\chi^2_n = 1.06$ and the WRMS is 1.07 mm/yr, which is considered to represent the best-fitting model. At the same time, the inversion calculation of $f = 3.7$ and $f = 4.1$ shows that the locking degree of the fault is basically consistent with the best-fitting model, indicating that the inversion results have good stability. To better illustrate the model selection and fitting effects, we drew the residual distribution of the best-fitting model (Figure 8). It can be seen from the figure that the direction of the residual distribution is random, and only a few sites have large residual GPS velocity values, whereas most stations inside the block and near the fault have small velocity residual values (<2 mm/yr). In addition, statistical analysis of the model-fitting residual distribution and internal strain residual of the block is also an important criterion for judging the quality of model inversion (Li et al., 2016). The statistical results of the velocity residual values conform to the Gaussian normal distribution; thus, the model is considered to be effective and the fitting results are good. Overall, the current model explains the GPS data and describes the seismic behavior of the northeastern margin of the Tibetan Plateau.

5.2 Seismic hazard analyses along the Qilian-Haiyuan fault zone

When an active fault is locked, it continuously accumulates energy under the action of stress. When it exceeds its stability limit, an earthquake occurs and releases energy, which then enters the next seismic cycle (Wallace et al., 2004; Zhang et al., 2013a; Qiu and Qiao, 2017). To analyze the seismic hazards of the Qilian–Haiyuan fault zone in the future, we studied the seismic hazards of each segment of the fault on the basis of the data of the fault locking degree and occurrence of small earthquakes.

In the eastern segment of the Tuolaishan fault, the intersection of the Tuolaishan fault and the Lenglongling fault, and the western segment of the Jinqianghe fault, the locking degree is strong, the locking depth and slip rate deficit (>5 mm/yr) are large, and the distribution of small earthquakes is low, indicating that the energy accumulation of these fault segments is fast, and the seismic hazard is high in the future. The eastern segment of the Lenglongling fault has strong locking and shows a low frequency of small earthquakes, but its locking

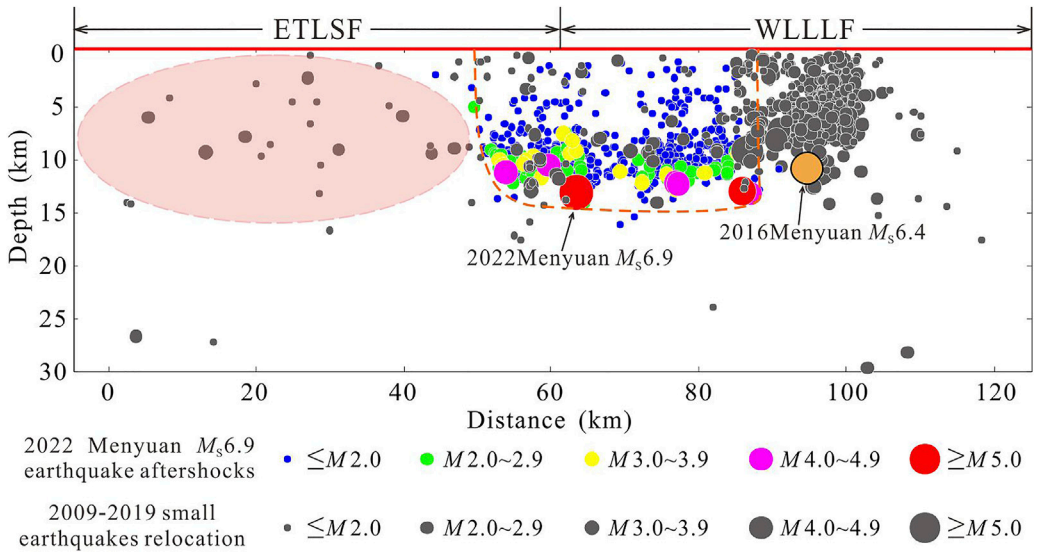

FIGURE 9
Profile of the 2009–2019 small earthquakes relocation (colored circles) and 2022 Menyuan M_S6.9 earthquake aftershocks (gray circles). Location of profile is shown in Figure 7. The pink ellipse corresponds to area of high risk for future earthquake. ETLSF: eastern segment of the Tuolaishan fault; WLLLF: western segment of the Lenglongling fault.

depth is low (only 6 km); the degree of locking in this segment may be increasing, and the seismic hazard here is moderate. The shallow region of the Maomaoshan fault has a high degree of locking, the locking degree is only 0.5 at the deep region of this fault. The distribution of small earthquakes was less, the current energy accumulation rate of the fault was relatively slow, the slip rate deficit was only 2–3 mm/yr, and the seismic hazard was moderate. The middle and western segments of the Tuolaishan, Laohushan, and Haiyuan faults are weakly locked, with a small locking depth, low slip rate deficit, and high frequency of earthquakes, indicating that these fault segments show frequent seismic activity, a weak energy accumulation level, and a low seismic hazard.

To analyze the impact of the 2022 Menyuan M_S6.9 earthquake on the future seismicity of the fault, we collected the relocation results of aftershocks within 9 days after the earthquake (Fan et al., 2022), and the regions located within 60 km on each side of the earthquake epicenter (black dotted box in Figure 7) was selected to plot the profile of the 2009–2019 small earthquakes relocation and 2022 Menyuan M_S6.9 earthquake aftershocks (Figure 9). It can be seen that the aftershocks are mainly distributed between a depth of 5–15 km, and the aftershocks occurred mainly between the western segment of the Lenglongling fault and the eastern segment of the Tuolaishan fault, with a length of approximately 40 km, consistent with other research results (Xu et al., 2022; Yang et al., 2022), which is longer than the surface rupture zone (20 km) observed in a field geological survey. Combined with the focal mechanism data of the 2022 Menyuan M_S6.9 earthquake and the distribution of aftershocks, we assume that the Lenglongling and Tuolaishan faults will be connected to a large strike-slip fault under the influence of this earthquake. Based on the InSAR coseismic deformation field and optical remote sensing interpretation, it was also found that the surface rupture caused by the earthquake extended to the Tuolaishan fault (Li et al., 2022; Yang et al., 2022). In addition, aftershocks were distributed on the Lenglongling fault and stopped at the location of the 2016 Menyuan M_S6.4earthquake, indicating that the middle segment of the Lenglongling fault, which has experienced an earthquake, is still in the post-earthquake adjustment phase, and the occurrence of aftershocks cannot continue without the accumulation of stress. Compared with the relocation distribution of small earthquakes from 2009 to 2019, the aftershocks of this earthquake filled the gap of small earthquakes in this segment and continued to migrate westward along the 2016 Menyuan M_S6.4earthquake. It is found that there is a seismic gap with a length of about 50 km in the eastern segment of the Tuolaishan fault to the west of the aftershock distribution. If the Tuolaishan and Lenglongling faults are connected, the next strong earthquake may migrate westward from the Lenglongling fault to the Tuolaishan fault, this segment is strongly locked and shows a high slip rate deficit, similar to the characteristics observed before the 2022 Menyuan M_S6.9 earthquake. Moreover, Xu et al. (2022) hypothesized that there is still some stress accumulation in this area, and thus, a risk of strong earthquakes. Therefore, more attention needs to be paid to the eastern segment of the Tuolaishan fault.

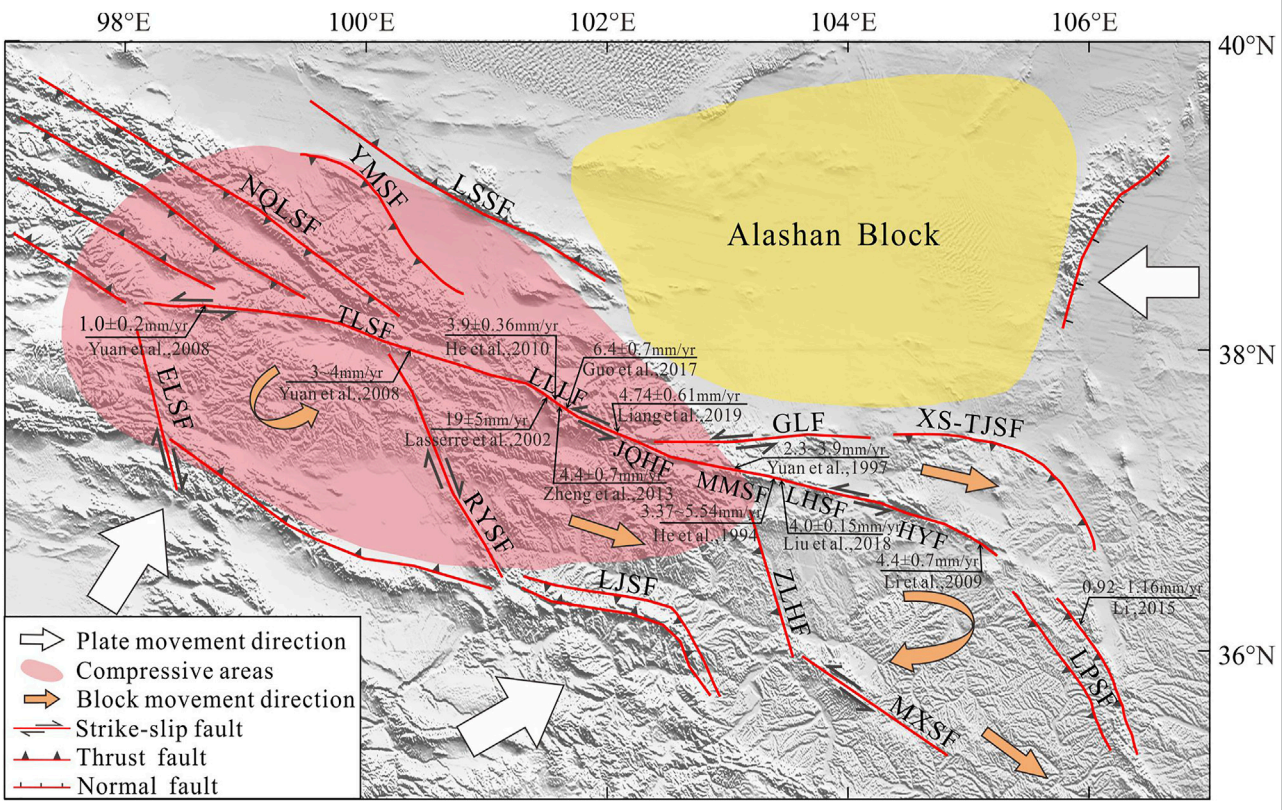

FIGURE 10
Tectonic transformation pattern in the northeastern margin of the Tibetan Plateau (modified from Yuan et al. (2004) and Zheng et al. (2013)). Red lines represent fault lines. White arrows represent the plate movement direction. Orange arrows represent the block movement direction. Pink shadow represents the compressive area. Yellow shadow represents the blocking area. LSSF: Longshoushan fault; YMSF: Yumushan fault; NQLSF: Northern Qilian Shan fault; TLSF: Tuolaishan fault; LLLF: Lenglongling fault; JQHF: Jinqianghe fault; MMSF: Maomaoshan fault; LHSF: Laohushan fault; HYF: Haiyuan fault; GLF: Gulang fault; XS–TJSF: Xiangshan–Tianjingshan fault; LPSF: Liupanshan fault; ELSF: Elashan fault; RYSF: Riyueshan fault; LJSF: Lajishan fault; ZLHF: Zhuanglanghe fault; MXSF: Maxianshan fault.

5.3 Regional crustal deformation model

The fault slip rate can not only reflect the most recent behavior of fault movement, but also reflect the main features of regional dynamics (Zhang et al., 2004; Gan et al., 2007; Zhang et al., 2013b). Several previous studies regarding the strike-slip rate of the Qilian–Haiyuan fault zone have been performed thus far; the geological slip rates reported in these studies vary greatly, showing a maximum value of 19 ± 5 mm/yr (Lasserre et al., 1999). The reliability of these results is controversial (Zheng et al., 2013; Guo et al., 2017), however, most studies have reported that the geological slip rate ranges from 4 to 6 mm/yr (He et al., 1994, 2010; Yuan et al., 1997, 2008; Li et al., 2009; Guo et al., 2017; Liu et al., 2018; Liang et al., 2019). The results obtained using geodetic data show that the slip rate ranges from2 to 8 mm/yr (Thatcher, 2007; Cavalié et al., 2008; Duvall and Clark, 2010; Loveless and Meade, 2010; Zheng et al., 2013; Li et al., 2016). However, the fault slip rate obtained in this study is mainly between 3.9 and 4.3 mm/yr, which is basically consistent with, or slightly smaller than, the strike-slip rates reported in most geological and geodetic studies. It can be considered that the present movement of the Qilian–Haiyuan fault zone is basically consistent with the characteristics of geological long-term movement, the fault activity has a good inheritance, and the main segment of the fault maintains a strike-slip rate of 4 mm/yr, indicating that the overall motion of the fault is consistent and corresponds to the concentration of the maximum shear strain rate in the Qilian–Haiyuan fault zone, while the strike-slip rate decreases rapidly at both ends of the fault (Yuan et al., 2008; Li, 2015). Furthermore, the motion characteristics of this strike-slip fault are similar to those reported in previous studies (Dawers et al., 1993; Duvall and Clark, 2010; Harkins et al., 2010; Zheng et al., 2013). Many studies have discussed strike-slip rates on the Qilian–Haiyuan fault, but only a few studies have summarized the vertical components of slip rates (and shortening rates). In accordance with the GPS results discussed above, the compressional rate of the Qilian–Haiyuan fault zone

decreases from 2.9 mm/yr in the western segment to about 1 mm/yr in the eastern segment, these results are consistent with the dilatation rates observed. At the same time, there was good correspondence with the topography observed. The west side is dominated by high-altitude mountains due to strong compression, whereas the east side is dominated by low-altitude basins due to weak compression. This indicates that the fault compressional rate may be related to crustal shortening (formation basin and uplifted mountain).

Based on the above characteristics, we discuss the regional current crustal deformation patterns. Under the dual action of the NE pushing of the Tibetan Plateau and the blocking of the Alashan block, strong tectonic deformation occurred in the northeastern margin of the Tibetan Plateau, and the direction of crustal movement was clockwise (Yuan et al., 2004). The Qilian Shan area is mainly subjected to strong compression, which results in the bending and rupture of strata and the formation of the Qilian fold system. There is obvious crustal shortening movement from the Elashan fault to the Yumushan fault, this is also affected by the interactions of block rotation and faults with different properties in the region and the transformation of the block rotations (Duvall and Clark, 2010; Ge et al., 2013) from the Qilian Shan to the east along the northeastern margin of the Tibetan Plateau. The crustal shortening rate gradually decreases, and the range of compression deformation also decreases. There is no obvious crustal shortening near the Haiyuan fault, which is a good explanation for the NE pushing being mainly distributed and absorbed by thrust faults, crustal thickening, and locally high marginal mountains. The decrease in the slip rate suggests that the boundary fault does not transfer a significant portion of the convergence between India and Asia out of India's path into Eurasia but merely redistributes the crustal thickening. The regional left-lateral strike-slip rate is mainly concentrated in the Qilian–Haiyuan fault zone, the strike-slip rate of each segment is basically the same, while the strike-slip movement of the other faults is not strong (the strike-slip rates for most of the faults are less than 1 mm/yr), indicating that the present-day crustal deformation in the northeastern margin of the Tibetan Plateau is mainly distributed in the shortened region of the crust on the Qilian Shan area and left-lateral strike-slip localized on the Qilian–Haiyuan fault zone (Figure 10).

6 Conclusion

In the paper, we used the GPS velocity field results from 2015 to 2021 and a negative dislocation program to invert the fault locking degree and the slip rate deficit, we obtained data regarding the current slip rate and strain rate field in the Qilian–Haiyuan fault zone. Combined with the results of the analysis of the relocation of small earthquakes, the characteristics of this fault zone before the 2022 Menyuan M_S6.9 earthquake were studied, the future seismic hazards of each segment of this fault zone were analyzed, and the regional crustal deformation pattern is discussed. The results are as follows:

(1) Before the 2022 Menyuan M_S6.9 earthquake, the dilatation rate at the seismogenic location was small, while the maximum shear strain rate was high (24×10^{-9}/yr). The seismogenic fault was strongly locked, the locking depth was deep, the slip rate deficit was large, and the distribution of small earthquakes was relatively few, which indicates that these characteristics are closely related to the occurrence of strong earthquakes. In addition, according to the aftershock relocation results, it is believed that the earthquake may link the Lenglongling and Tuolaishan faults into a large strike-slip fault.
(2) The eastern segment of the Tuolaishan fault is strongly locked, with high locking depth and large slip rate deficit, and the distribution of small earthquakes is few, combined with the small earthquakes and the locking degree before the 2022 Menyuan M_S6.9 earthquake, indicate that the eastern segment of the Tuolaishan fault is highly likely to have strong earthquake in the future, which requires further attention.
(3) The strike-slip rate of the Qilian–Haiyuan fault zone is mainly between 3.9 and 4.3 mm/yr, the overall movement of the fault is consistent, and the compressional rate gradually decreases from 2.9 mm/yr in the western segment to 1 mm/yr in the eastern segment, the compressional rate of the fault may be related to crustal shorting (formation basin and uplift mountain). Therefore, the present-day crustal deformation in the northeastern margin of the Tibetan Plateau is mainly distributed in the shortened region of the crust on the Qilian Shan and the left-lateral strike-slip localized on the Qilian–Haiyuan fault zone.

Data availability statement

The original contributions presented in the study are included in the article/supplementary material, further inquiries can be directed to the corresponding author.

Author contributions

LL: Conceived this research, Writing - original draft; editing, WZ: GPS data processing LJ: Guide and supervision. LZ: Methodology, Block Model FJ: Strain Rate Field. All authors reviewed and supervised the manuscript and approved it for publication.

Acknowledgments

We are grateful to McCaffrey for permitting us to use of the TDEFNODE software. We would like to thank professor Fang Lihua and Long Feng for providing relocation results of aftershocks and

small earthquakes. Some figures and maps were prepared using Generic Mapping Tools software (Wessel et al., 2013).

Conflict of interest

The authors declare that the research was conducted in the absence of any commercial or financial relationships that could be construed as a potential conflict of interest.

Publisher's note

References

Altamimi, Z., Métivier, L., Rebischung, P., Rouby, H., and Collilieux, X. (2017). ITRF2014 plate motion model. *Geophys. J. Int.* 209, 1906–1912. doi:10.1093/gji/ggx136

Cavalié, O., Lasserre, C., Doin, M. P., Peltzer, G., Sun, J., Xu, X., et al. (2008). Measurement of interseismic strain across the Haiyuan fault (Gansu, China), by InSAR. *Earth Planet. Sci. Lett.* 275 (3-4), 246–257. doi:10.1016/j.epsl.2008.07.057

Daout, S., Jolivet, R., Lasserre, C., Doin, M. P., Barbot, S., Tapponnier, P., et al. (2016). Along-strike variations of the partitioning of convergence across the Haiyuan fault system detected by InSAR. *Geophys. J. Int.* 205 (1), 536–547. doi:10.1093/gji/ggw028

Dawers, N. H., Anders, M. H., and Scholz, C. H. (1993). Growth of normal faults: displacement length scaling. *Geology* 17, 607–614. doi:10.1130/0091-7613(1993)021<1107:GONFDL>2.3.CO;2

Dewey, J. F., and Burke, K. C. A. (1973). Tibetan, variscan, and precambrian basement reactivation: Products of continental collision. *J. Geol.* 81, 683–692. doi:10.1086/627920

Duvall, A. R., and Clark, M. K. (2010). Dissipation of fast strike-slip faulting within and beyond northeastern Tibet. *Geology* 38 (3), 223–226. doi:10.1130/G30711.1

England, P., and Houseman, G. (1986). Finite strain calculations of continental deformation: 2. Comparison with the India-Asia collision zone. *J. Geophys. Res.* 91 (B3), 3664–3676. doi:10.1029/jb091ib03p03664

Fan, L. P., Li, B. R., Jiang, C., Liao, S. R., and Fang, L. H. (2022). Precise relocation of the 2 aftershock sequences of the 2022 *M*6.9 Menyuan earthquake. *Earthquake Sciecne* 35 (2), 138–145. doi:10.13140/RG.2.2.19922.07367

Gan, W. P., Zhang, P. Z., Shen, Z. K., Niu, Z. J., Wang, M., Wan, Y. G., et al. (2007). Present- day crustal motion within the Tibetan Plateau inferred from GPS measurements. *J. Geophys. Res.* 112, B08416. doi:10.1029/2005JB004120

Gao, W. (2018). *Late quaternary activity of the Tianqiaogou-Huangyangchuan fault: Implication for the tectonic movement mechanism at the northeastern Tibet*. Beijing: Institute of Geology, China Earthquake Administration.

Gaudemer, Y., Tapponnier, P., Peltzer, G., Meyer, B., Guo, S., Chen, Z., et al. (1995). Partitioning of crustal slip between linked, active faults in the eastern Qilian Shan, and evidence for a major seismic gap, the 'Tianzhu gap', on the Western Haiyuan Fault, Gansu (China). *Geophys. J. Int.* 120 (3), 599–645. doi:10.1111/j.1365-246X.1995.tb01842.x

Ge, W. P., Wang, M., Shen, Z. K., Yuan, D. Y., and Zheng, W. J. (2013). Intersiesmic kinematics and defromation patterns on the upper crust of Qaidam-Qilianshan block. *Chin. J. Geophys. (in Chinese)* 56 (9), 2994–3010. doi:10.6038/cjg20130913

Guo, P. (2019). *Earthquake recurrence behavior and seismic hazards of the Lenglongling fault, northern qilian Shan*. Beijing: Institute of Geology, China Earthquake Administration.

Guo, P., Han, Z. J., Jiang, W. L., and Mao, Z. B. (2017). Holocene left-lateral slip rate of the Lenglongling fault, northeastern margin of the tibetan plateau. *Seismology and Geology (in Chinese)* 39 (2), 323–341. doi:10.3969/j.issn.0253-4967.2017.02.005

Han, Z. J., Dong, S. P., Xie, F. R., and An, Y. F. (2008). Earthquake triggering by static stress: the 5 major earthquakes with *M*≥7 (1561~1920) in the northern section of south-north seismic zone. China. *Chin. J. Geophys (in Chinese)* 51 (6), 1776–1784.

Hao, M., Li, Y. H., and Qin, S. L. (2017). Spatial and temporal distribution of slip rate deficit across Haiyuan-Liupan Shan fault zone constrained by GPS data. *Seismology and Geology (in Chinese)* 39 (3), 471–484. doi:10.3969/j.issn.0253-4967.2017.03.003

Harkins, N., Kirby, E., Shi, X., Wang, E., Burbank, D., Chun, F., et al. (2010). Millennial slip rates along the eastern Kunlun fault: implications for the dynamics of intracontinental deformation in Asia. *Lithosphere* 2, 247–266. doi:10.1130/L85.1

Hashimoto, C., Noda, A., Sagiya, T., and Matsu'Ura, M. (2009). Interplate seismogenic zones along the Kuril Japan trench inferred from GPS data inversion. *Nat. Geosci.* 2 (2), 141–144. doi:10.1038/ngeo421

He, W. G., Liu, B. C., Lu, T., Yuan, D., Liu, J. S., and Liu, X. F. (1994). Study on the segmentation of Laohushan fault zone. *Northwestern Seismological Journal (in Chinese)* 16 (3), 66–72.

He, W. G., Yuan, D. Y., Ge, W. P., and Luo, H. (2010). Determination of the slip rate of the Lenglongling Fault in the middle and eastern segments of the Qilian Mountain active fault zone. *Earthquake (in Chinese)* 30 (1), 131–137. doi:10.1017/S0004972710001772

Herring, T. A., King, R. W., and McClusky, S. C. (2015). *GAMIT reference manual, GPS analysis at MIT*. Release 10.6. Cambridge, MA: Massachusetts Institute of Technology.

Jolivet, R., Lasserre, C., Doin, M. P., Guillaso, S., Peltzer, G., Dailu, R., et al. (2012). Shallow creep on the Haiyuan fault (Gansu, China) revealed by SAR interferometry. *J. Geophys. Res.* 117 (B6), 137–147. doi:10.1029/2011JB008732

Jolivet, R., Lasserre, C., Doin, M. P., Peltzer, G., Avouac, J. P., Sun, J., et al. (2013). Spatio-temporal evolution of aseismic slip along the Haiyuan fault, China: implications for fault frictional properties. *Earth and Planetary Science Letters* 377-378, 23–33. doi:10.1016/j.epsl.2013.07.020

Lasserre, C., Morel, P. H., Gaudemer, Y., Tapponnier, P., Ryerson, F. J., King, G. C. P., et al. (1999). Post glacial Left slip-rate and past occurrence of *M* > 8 earthquakes on Western Haiyuan fault, Gansu, China. *J. Geophys. Res.* 104 (B8), 17633–17651. doi:10.1029/1998JB900082

Li, C. Y., Zhang, P. Z., Yin, J. H., and Min, W. (2009). Late Quaternary left-lateral slip rate of the Haiyuan Fault, northeastern margin of the Tibetan plateau. *Tectonics* 28 (5), TC5010. doi:10.1029/2008tc002302

Li, J. Y., Zhou, B. G., Li, T. M., Yang, Y. L., Li, Z. F., and Long, F. (2020). Seismogenic depths of the Anninghe-Zemuhe and Daliangshan fault zones and their seismic hazards. *Chin. J. Geophys (in Chinese)* 63 (10), 3669–3682. doi:10.6038/cjg2020N0201

Li, Q., Jiang, Z. S., Wu, Y. Q., and Zhao, J. (2014). Inversion of locking and distribution of slip deficit in Haiyuan-Liupan fault zone using GPS data. *Geomatics and Information Science of Wuhan University* 39 (5), 575–580. (in Chinese). doi:10.13203/j.whugis2012161

Li, X. Q. (2015). *Activity of the Eastern Liupanshan piedmot fault zone since late Quaternary*. Beijing: Institute of Earthquake Science, China Earthquake Administration.

Li, Y. C., Shan, X. J., Qu, C. Y., and Wang, Z. J. (2016). Fault locking and slip rate deficit of the Haiyuan-Liupanshan fault zone in the northeastern margin of the Tibetan Plateau. *Journal of Geodynamics* 102, 47–57. doi:10.1016/j.jog.2016.07.005

Li, Y. H., Cui, D. X., and Hao, M. (2015). GPS constrained inversion of slip rate on major active faults in the northeastern margin of Tibet plateau. *Earth Sci.* 40 (10), 1767. doi:10.3799/dqkx.2015.158

Li, Z. H., Han, B. Q., Liu, Z. J., Zhang, M. M., Yu, C., Chen, B., et al. (2022). Source parameters and slip distributions of the 2016 and 2022 Menyuan, Qinghai earthquakes constrained by InSAR observations. *Geomat. Inf. Sci.*

Wuhan Univ. 47 (6), 887–897. (in Chinese). doi:10.13203/j.whugis20220037

Liang, S. M., Zheng, W. J., Chen, G., and Zhang, P. Z. (2019). "Late Quaternary movement characteristics and tectonic significance of Jinqianghe of Qilian-Haiyuan fault zone," in Annual meeting of Chinese Geoscience Union 2019 (Beijing: CGU).

Liu, J. R., Ren, Z. K., Zhang, H. P., Li, C. Y., Zhang, Z. Q., Zheng, W. J., et al. (2018). Late Quaternary slip rate of the Laohushan fault with in the Haiyuan fault zone and its tectonic implications. *Chin. J. Geophys (in Chinese)* 61 (4), 1281–1297. doi:10.6038/cjg2018L0364

Liu, L., Jiang, F. Y., and Zhu, L. Y. (2020). Characteristics of recent crustal movement and seismicity in the Northern section of the North-south seismic belt. *Journal of Seismological Research (in Chinese)* 43 (4), 658–665. doi:10.3969/j.issn.1000-0666.2020.04.008

Loveless, J. P., and Meade, B. J. (2010). Geodetic imaging of plate motions, slip rates, and partitioning of deformation in Japan. *J. Geophys. Res.* 115 (B2), B02410. doi:10.1029/2008JB006248

Loveless, J. P., and Meade, B. J. (2011). Spatial correlation of interseismic coupling and coseismic rupture extent of the 2011 M_W=9.0 Tohoku-Oki earthquake. *Geophys. Res. Lett.* 3 (17), L17306. doi:10.1029/2011GL048561

Madariaga, R., Métois, M., Vigny, C., and Campos, J. (2010). Central Chile finally breaks. *Science* 328 (5975), 181–182. doi:10.1126/science.1189197

Mao, A. L., Harrison, C. G. A., and Dixon, T. H. (1999). Noise in GPS coordinate time series. *J. Geophys. Res.* 104 (B2), 2797–2816. doi:10.1029/1998JB900033

McCaffrey, R. (2005). Block kinematics of the Pacific-north America plate boundary in the southwestern United States from inversion of GPS, seismological, and geologic data. *J. Geophys. Res.* 110 (B7), B07401. doi:10.1029/2004jb003307

McCaffrey, R. (2002). *Crustal block rotation sand plate coupling*. Plate Boundary Zones. Washington, DC: AGU, 101–122. doi:10.1029/GD030p0101

McCaffrey, R., Qamar, A. I., King, R. W., Wells, R., Khazaradze, G., Williams, C. A., et al. (2007). Fault locking, block rotation and crustal deformation in the Pacific Northwest. *Geophys. J. Int.* 169, 1315–1340. doi:10.1111/j.1365-246X.2007.03371.x

McCaffrey, R. (2009). Time-dependent inversion of three-component continuous GPS for steady and transient sources in northern Cascadia. *Geophys. Res. Lett.* 36, L07304. doi:10.1029/2008GL036784

Meng, G. J., Shen, X. H., Vladimir, S., Eugene, A. R., and Wu, J. C. (2009). Research on characteristics of present-day crustal motion and deformation in Kamchatka area. *Chinese J. Geophys.* 52 (3), 390–402. doi:10.1002/cjg2.1359

Métivier, F., Gaudemer, Y., Tapponnier, P., and Meyer, B. (1998). Northeastward growth of the Tibet plateau deduced from balanced reconstruction of two depositional areas: The Qaidam and Hexi Corridor basins, China. *Tectonics* 17, 823–842. doi:10.1029/98TC02764

Molnar, P., and Stock, J. M. (2009). Slowing of India's convergence with Eurasia since 20Ma and its implications for Tibetan mantle dynamics. *Tectonics* 28, Art No TC3001. doi:10.1029/2008TC002271

Moreno, M., Rosenau, M., and Oncken, O. (2010). 2010 Maule earthquake slip correlates with pre-seismic locking of Andean subduction zone. *Nature* 467 (7312), 198–202. doi:10.1038/nature09349

Peltzer, G., and Tapponnier, P. (1988). formation and evolution of strike slip faults, rifts, and basins during the India-Asia collision: an experimental approach. *J. Geophys. Res.* 93 (B12), 15085–15117. doi:10.1029/JB093iB12p15085

Qiu, J. T., and Qiao, X. J. (2017). A study on the seismogenic structure of the 2016 Zaduo, Qinghai M_s6. 2 earthquake using InSAR technology. *Geod. Geodyn.* 8 (5), 342–346. doi:10.1016/j.geog.2017.04.008

Schmittbuhl, J., Karabulut, H., Lengline, O., and Bouchon, M. (2015). Seismicity distribution and locking depth along the main marmara fault, Turkey. *Geochem. Geophys. Geosyst.* 17 (3), 954–965. doi:10.1002/2015GC006120

Shen, Z. K., Wang, M., Zeng, Y. H., and Wang, F. (2015). Optimal interpolation of spatially discretized geodetic data. *Bulletin of The Seismological Society of America* 105 (4), 2117–2127. doi:10.1785/0120140247

Song, S. W., Li, Y. H., and Hao, M. (2022). Active crustal deformation model of the Fen - Wei rift zone, North China: Integration of geologic, geodetic, and stress direction datasets. *Front. Earth Sci.* 10, 964800. doi:10.3389/feart.2022.964800

Tapponnier, P., and Molnar, P. (1976). Slip-line field theory and large scale continental tectonics. *Nature* 264 (5584), 319–324. doi:10.1038/264319a0

Tapponnier, P., Xu, Z. Q., Roger, F., Meyer, B., Arnaud, N., Wittlinger, G., et al.(2001). Oblique stepwise rise and growth of the tibet plateau. *Science* 294 (5547), 1671–1677. doi:10.1126/science.105978

Thatcher, W. (2007). Microplate model for the present-day deformation of Tibet. *J. Geophys. Res.* 112 (B1), B01401. doi:10.1029/2005JB004244

Wallace, L. M., Beavan, J., McCaffrey, R., Darby, D., Loratung, W., Hasiata, S., et al. (2004). GPS and seismological constraints on active tectonics and arc-continent collision in Papua New Guinea: Implications for mechanics of microplate rotations in a plate boundary zone. *J. Geophys. Res.* 109 (B5), B05404. doi:10.1029/2003JB002481

Wang, H., Liu, M., Cao, J. L., Shen, X. H., and Zhang, G. M. (2011). Slip rates and seismic moment deficits on major active faults in mainland China. *J. Geophys. Res.* 116 (B2), B02405. doi:10.1029/2010JB007821

Wang, K. L., Wells, R., Mazzotti, S., Hyndman, R. D., and Sagiya, T. (2003). A revised dislocation model of inter seismic deformation of the Cascadia subduction zone. *J. Geophys. Res.* 108 (B1). doi:10.1029/2001JB001227

Wang, M., and Shen, Z. K. (2020). Present-day crustal deformation of continental China derived from GPS and its tectonic implications. *J. Geophys. Res. Solid Earth* 125, e2019JB018774. doi:10.1029/2019JB018774

Wang, W., Yang, S. M., and Wang, Q. (2009). Crustal block rotations in Chinese mainland revealed by GPS measurements. *Earthq. Sci.* 22 (6), 639–649. doi:10.1007/s11589-009-0639-4

Wessel, P., Smith, W. H., Scharroo, R., Luis, J., and Wobbe, F. (2013). Generic mapping Tools: Improved version released. *Eos Trans. AGU.* 94 (45), 409–410. doi:10.1002/2013EO450001

Wiemer, S., and Wyss, M. (1997). Mapping the frequency-magnitude distribution in asperities: An improved technique to calculate recurrence times? *J. Geophys. Res.* 1021 (B7), 15115–15128. doi:10.1029/97JB00726

Wyss, M., and Wiemer, S. (2000). Change in the probability for earthquakes in southern California due to the Landers magnitude 7.3 earthquake. *Science* 290, 1334–1338. doi:10.1126/science.290.5495.1334

Xu, Y. C., Guo, X. Y., and Feng, L. L. (2022). Relocation and focal mechanism solutions of the M_S6.9 Menyuan earthquake sequence on January 8, 2022 in Qinghai Province. *Acta Seismologica Sinica* 44 (2), 195–210. doi:10.11939/jass.20220008

Yang, G. H., Li, Y. X., Han, Y. P., Hu, X. K., and Gong, R. M. (2002). Current horizontal strain field in Chinese mainland derived from GPS data. *Acta Seimol. Sin.* 24 (4), 351–362. doi:10.1007/s11589-002-0028-8

Yang, H. F., Wang, D., Guo, R. M., Xie, M. Y., Zang, Y., Wang, Y., et al. (2022). Rapid report of the 8 january 2022 M_S 6.9 Menyuan earthquake, Qinghai, China. *Earthquake Research Advances* 2 (1), 100113. doi:10.1016/j.eqrea.2022.100113

Yuan, D. Y., Liu, B. C., Lu, T. Y., He, W. G., and Liu, X. F. (1997). Slip rates of the Maomaoshan fault zone in Gansu province obtainted by using ages of loess-palaeosol sequence. *Seismology and Geology (in Chinese)* 19 (001), 1–8. doi:10.1063/1.1680233

Yuan, D. Y., Zhang, P. Z., Ge, W. P., Liu, X. J., Zhang, H., and Liang, M. (2008). "Late Quaternary strike-slip features along the Western segment of Haiyuan-Qilianshan Fault, NE Tibetan plateau," in American Geophysical Union, Fall Meeting 2008 (San Francisco, CA: AGU).

Yuan, D. Y., Zhang, P. Z., Liu, B. C., Gan, W. J., Mao, F. Y., Wang, Z. C., et al. (2004). Geometrical imagery and tectonic transformation of Late Quaternary active tectonics in northeastern margin of Qinghai-Xizang Plateau. *Acta Geologica Sinica (in Chinese)* 78 (2), 270–278. doi:10.3321/j.issn:0001-5717.2004.02.017

Zhan, Y., Zhao, G. Z., Chen, X. B., Tang, J., Wang, J. J., and Deng, Q. H. (2004). Crustal structure from magnetotelluric profiling in the Haiyuan earthquake area, Ningxia hui autonomous region, China. *Chin. J. Geophys (in Chinese)* 47 (2), 274–281.

Zhang, P. Z., Deng, Q. D., Zhang, G. M., Ma, J., Gan, W. J., Min, W., et al. (2003). Active tectonic blocks and strong earthquakes in the continent of China. *Science in China (Series D) (in Chinese)* 33 (S1), 12–20. doi:10.3969/j.issn.1674-7240.2003.z1.002

Zhang, P. Z., Deng, Q. D., Zhang, Z. Q., and Li, H. B. (2013a). Active faults, earthquake hazards and associated geodynamic processes in continental China. *Sci. Sin. -Terrae.* 43 (10), 1607–1620. doi:10.1360/zd-2013-43-10-1607

Zhang, P. Z., Gan, W. J., Shen, Z. K., and Wang, M. (2005). A coupling model of rigid-block movement and continuous deformation: Patterns of the present-day deformation of China's continent and its vicinity. *Acta Geologica Sinica* 79 (06), 748–756. doi:10.3321/j.issn:0001-5717.2005.06.004

Zhang, P. Z., Shen, Z. K., Wang, M., Gan, W. J., Bürgmann, R., Wang, Q., et al.(2004). Continuous deformation of the Tibetan Plateau from global positioning system data. *Geol.* 32 (9), 809. doi:10.1130/G20554.1

Zhang, Z. Q., McCaffrey, R., and Zhang, P. Z. (2013b). Relative motion across the eastern Tibetan plateau: Contributions from faulting, internal strain and rotation rates. *Tectonophysics* 584, 240–256. doi:10.1016/j.tecto.2012.08.006

Zhao, J., Jiang, Z. S., Niu, A. F., Wu, Y. Q., Zhan, W., Wu, W. X., et al. (2017). Characteristics of fault locking and fault slip deficit in the main Himalaya thrust fault. *Geomatics and Information Science of Wuhan University* 42 (12), 9. (in Chinese). doi:10.13203/j.whugis20150619

Zhao, J., Jiang, Z. S., Wu, Y. Q., Liu, X. X., Wu, W. X., and Li, Q. (2012). Study on fault locking and fault slip deficit of the Longmenshan fault zone before the Wenchuan earthquake. *Chin. J. Geophys (in Chinese)* 55 (09), 2963–2972. doi:10.6038/j.issn.0001-5733.2012.09.015

Zhao, J., Ren, J. W., Liu, J., Jiang, Z. S., Liu, X. X., Liang, H. B., et al. (2020). Coupling fraction and relocking process of the longmenshan fault zone following the 2008 *Mw*7.9 wenchuan earthquake. *Journal of Geodynamics* 137, 101730. doi:10.1016/j.jog.2020.101730

Zheng, W. J., Zhang, P. Z., He, W. G., Yuan, D. Y., Shao, Y. X., Zheng, D. W., et al.(2013). Transformation of displacement between strike-slip and crustal shortening in the northern margin of the Tibetan plateau: Evidence from decadal GPS measurements and late quaternary slip rates on faults. *Tectonophysics* 584 (1), 267–280. doi:10.1016/j.tecto.2012.01.006